

Project Number: ME-CF-LI07

DESIGN AND REALIZATION OF A LASER HOLOGRAPHIC OTOSCOPE

A Major Qualifying Project Report

Submitted to the Faculty

of the

WORCESTER POLYTECHNIC INSTITUTE

in partial fulfillment of the requirements for the

Degree of Bachelor of Science

in Mechanical Engineering

by

Benjamin W. Dwyer

Martin E. Maccaferri

Christian R. Wester

Date: 24 April, 2008

Keywords:

1. laser interferometry
2. tympanic membrane
3. holography

Professor Cosme Furlong

Abstract

Audiologists are in need of sophisticated analysis equipment with nanometer resolution that will provide comprehensive data with full field of view imaging of the ear's tympanic membrane. Technology capable of providing this data will significantly improve the treatment of patients. This report details the mechanical design and fabrication of a laser holographic otoscope created to meet these needs. The image quality from the constructed device has been validated and is being used in a real medical research environment to investigate different species of tympanic membranes, including that of humans.

Acknowledgments

We would like to acknowledge Professor Cosme Furlong for his guidance and efforts during the development of this project. Additionally, we would like to thank the graduate and post-graduate students of the Center for Holographic Studies and Laser micro-mechaTronics that handled the optical and software aspects of the overall system, as their efforts and knowledge established a necessary foundation for assessing and validating the design.

We would like to express our sincere appreciation to the faculty and staff of the Mechanical Engineering Department of Worcester Polytechnic Institute for their assistance regarding part procurement and general logistical inquiries. Additionally, we would like to extend thanks to the faculty and staff involved in managing the Washburn Shops of Worcester Polytechnic Institute. Allowing us to work independently enabled the project to develop as quickly as possible and was a key contributor to the success of the final product.

Table of Contents

Abstract.....	i
Acknowledgments.....	ii
Table of Contents.....	iii
List of Figures.....	iv
List of Tables.....	v
1 Introduction.....	1
2 Background.....	4
2.1 Tympanic Membranes.....	4
2.2 Medical Techniques and Procedures.....	6
2.3 State of the Art.....	8
2.4 Interferometers.....	9
3 Methodology.....	15
3.1 Optical Head Development.....	15
3.2 Validation of Performance.....	20
3.2.1 Analytical Results.....	20
3.2.2 Computational Results.....	25
3.2.3 Developing a Perfect Membrane.....	28
3.2.4 Experimental Results.....	32
3.2.5 Comparing Results.....	33
4 Results.....	36
5 Conclusions.....	38
6 References.....	39
7 Appendix A: Contents of Enclosed CD.....	41

List of Figures

Fig. 1 - Ear Anatomy (Csillag, 2005)	5
Fig. 2 - Example of an Interferometer (Answers.com).....	10
Fig. 3- Example of Principles of Holography (Stereoscopy.com).....	12
Fig. 4 - Ruby Laser Emitting Light, from http://science.howstuffworks.com/laser.htm ..	13
Fig. 5 - Breadboard Configuration.....	15
Fig. 6 - Cylindrical Design.....	16
Fig. 7 - Plate Design.....	17
Fig. 8 - Box Design.....	18
Fig. 9 - Refined Box Design	19
Fig. 10 - First Mode of Vibration Obtained with MathCAD	24
Fig. 11 - 3D Deformable Solid Thin Membrane.....	25
Fig. 12 - A Closer Look at Partitions.....	26
Fig. 13 - Refined Mesh	27
Fig. 14 - Fourth Mode Deformed Contour Plot	28
Fig. 15 – Foil Clamping Mechanism Mounted onto the Piezo.....	29
Fig. 16 - Deformations on a Creased Foil Due to Clamping	31
Fig. 17 - Live Chinchilla TM Excited at: 600Hz -23dBV (101dBSPL), 10 kHz - 29dBV (127 dBSPL), 22 kHz - 39dBV (108dBSPL)	36
Fig. 18 - Post Mortem Chinchilla TM Excited at 500Hz - 46dBV, 10 kHz - 34 dBV, and 22kHz - 29 dBV	37

List of Tables

Table 1 - Working Distance Constraints.....	17
Table 2 - Membrane Test Data	32
Table 3 - Mode Shapes and Frequencies for Modes 1 through 3 Taken from Experimental, Analytical and Finite Element Methods	33
Table 4 - Mode Shapes and Frequencies for Modes 4 through 6 Taken from Experimental, Analytical and Finite Element Methods	34
Table 5 - Experimental Results Percent Error	34

1 Introduction

Fast paced advances in medical technology have been resulting in more accurate tools designed to help medical professionals perform their jobs. Sophisticated medical equipment is applied in all aspects of the field from making diagnoses' to performing surgeries. The development of these devices requires current technology that can be used dependably time after time. One of the medical world's current areas of advanced development is in the knowledge on hearing conditions related to the functionality of the middle ear. One part of the middle ear that is commonly examined is the tympanic membrane. This particular portion of ear anatomy is of particular interest to medical researchers.

There are several methods for diagnosing hearing problems which have been used for many years by medical professionals, almost completely unchanged from their original method. Those who are on the cutting edge of audiology are looking to use the most modern technological advances to develop more sophisticated tools for diagnoses. One of the main areas of research towards this goal is in applying laser based technology for the purposes of collecting information.

One of the current areas of laser related research that has shown the ability to provide doctors with information on the state of a tympanic membrane is optoelectronic holography. This technology allows researchers to see real-time full field of view images of a sample object. The technology has the ability to view very small areas and observe minute deflections. This method varies from a related laser technology known as laser vibrometry, which relies on lasers to detect the characteristics of a sample's vibrations in

many different frequencies simultaneously. Laser vibrometry is based on point by point measurements, rather than that of full field of view.

The focus of this Major Qualifying Project is to package state of the art optical equipment that has been arranged for optoelectronic holography. The optical system is designed for fields of view on the order of 10 mm in diameter. At the outset of the project's development all optical testing was performed using optical tables, posts and mounts. These components provided maximum system flexibility, but required the user to be highly knowledgeable in the manipulation and application of the optical equipment. Conducting tests with the posts is overly time-consuming, and there are large uncertainties between different tests conducted once components in the system are modified or repositioned. Repeatability is also difficult to achieve under these conditions. The post mounts are also subject to vibrations which ruin image quality and reliability.

The goal of this Major Qualifying Project is to design and fabricate a packaged optical device to be used dependably with little technical training required on the part of the user. By designing the system to minimize variability in optical component positioning and maximal stability, the device is made to have maximal functionality with all samples. The challenges presented to the design team included the need to gain a greater understanding of the optical system, fabricating components with very fine tolerances, and accommodating all necessary degrees of freedom associated with the effective use of the medical device.

Along with the development of the medical device it is also necessary to verify that the system is working correctly and effectively. Because of the very fine

displacements which the optical equipment was designed to observe, a sophisticated testing system was needed. The accuracy of the testing was of extremely high importance to ensure consistency between results obtained using: finite element methods, analytical calculations and experimental data. It was found that small inconsistencies in the experimental system would cause noticeable disturbances in the experimental results. The challenge of developing an appropriate experimental set up was solved as well as the development of a practical optoelectronic holographic testing device.

2 Background

2.1 Tympanic Membranes

The human ear is a complicated organ that makes use of many different devices both mechanically and neurologically to produce both the sensation of hearing and that of equilibrium, (Csillag, 2005). Anatomy of the ear is normally separated by experts in to three main parts for the purpose of analyzation: the outer, middle and inner ears, (Csillag, 2005). The transfer of changes in air pressure between these separate sections of the ear is dependent on several different systems within the ear working in conjunction (Schubert, 1980). The inner ear both protects the inner two sections of the ear along with funneling sound waves into them as well, (Schubert, 1980). The middle ear turns fluid energy in to mechanical energy that is then transferred to the inner ear in distinct patterns which are based entirely on the external soundings, (Schubert, 1980). The inner ear receives the signals sent from outside and interacts neurologically with the mind via the vibration of hair follicles which are varied in length so as to react to different frequencies which they are exposed to, thus inducing different tones and pitches of sound, (Csillag, 2005). The magnitude with which the hairs react determines largely the volume of the noise which is heard, (Csillag, 2005).

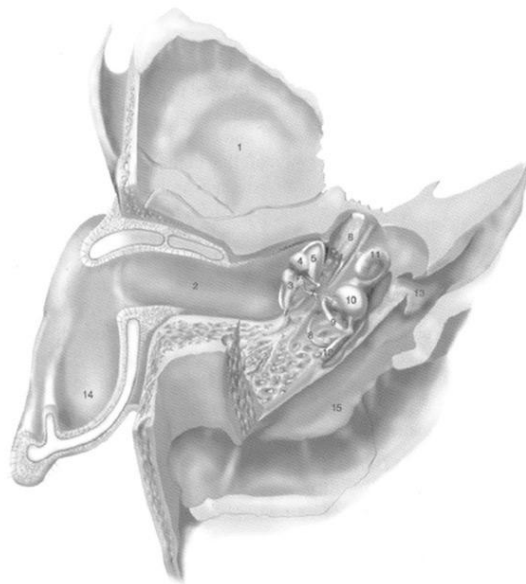


Fig. 1.1

Overview of the ear.

1. Squamous temporal
2. External auditory meatus
3. Malleus
4. Incus
5. Tympanic membrane
6. Pharyngotympanic tube
7. Stapes
8. Lateral semicircular canal
9. Anterior semicircular canal
10. Vestibule
11. Cochlea
12. Posterior semicircular canal
13. Internal auditory meatus
14. Pinna
15. Groove for sigmoid sinus

Fig. 1 - Ear Anatomy (Csillag, 2005)

When there is hearing loss or failure then the middle ear will frequently be investigated as to the cause of the condition. The middle ear consists of the tympanic membrane, space for fluid transfer and three small bones: the malleus, incus and stapes, (Schubert, 1980). The three bones function normally as the mechanical linkage that will transfer vibrations from the tympanic membrane in to the fluids of the inner ear, (Schubert, 1980). For the purposes of diagnosis, often times hearing loss is found to be conductive, or that it is due to a disruption in the mechanical system that makes up the middle ear, (Schubert, 1980). There are many different breakdowns in the function of the middle ear that are seen by doctors in their practices, such as: tympanic membrane perforation, incus necrosis, myringostapediopexy, malleus head fixation, tympanosclerosis, cholesteatoma, polyps, serous otitis media, otosclerosis and trauma,

(Katz, 1994). These conditions stem mainly from the presence of infection within the middle ear but can be caused by many different factors, (Katz, 1994).

2.2 Medical Techniques and Procedures

For diagnosis of conditions of the middle ear there are not many different methods used in practice. The field of tympanometry was developed by doctors once it was determined that the function of the tympanic membrane is dependent on the entire mechanical system that makes up the middle ear, (Schubert, 1980). The tympanic membrane acts as the boundary between where doctors have decided the outer and middle ear is located, and is therefore the most readily accessible part of middle ear anatomy, (Schubert, 1980). The tympanic membrane exhibits the signs of conductive hearing conditions due to malfunction in the middle ear, as the entire system is interconnected, (Schubert, 1980). Tympanometry is the technique used to extract data based on the behavior of the tympanic membrane, (Katz, 1994).

Traditional Tympanometry is a process that gives indirect data about the level of “impedance” demonstrated by tympanic membrane, (Schubert, 1980). Impedance is in effect related to the “stiffness” of the tympanic membrane, which is what the physicians are testing in actuality, (Schubert, 1980). To better ensure that the loss in hearing is indeed conductive professionals will use a bone vibrator to make sure that the difficulty does not instead lay with the inner ear, (Schubert, 1980). This device induces the sensation of hearing by vibrating the skull around the inner ear rather than rely on the middle ear to transmit the information, (Schubert, 1980). If the patient shows signs of

hearing as they should have via sound wave propagation then there is a very good sign that the middle ear is responsible for the condition, (Schubert, 1980). Doctors induce different pressures in the ear canal and take measurements with relation to available volumes, (Schubert, 1980). If the volumes recorded are found to differ from that of the normal ear then it is even further likely that there is a problem in the middle ear, (Schubert, 1980). The type of pattern detected can also lead doctors to determine what type of middle ear condition the patient has, enabling them to begin determining treatment, (Katz, 1994). This type of analysis combined with visual inspection per use of an otoscope provides the information needed for doctors to make proper diagnosis of particular ear problems, (Katz, 1994). The testing procedures require many different types of specialization and require a large time investment on the part of the patient and doctor.

There are problems involved with these testing methods that create certain unknowns that make the time consuming diagnoses still lack absolute certainty, (Katz, 1994). One such variable is the inconsistency in tympanic membrane response purely based on the tones emitted by microphones, (Schubert, 1980). This response needs to be filtered so as not to disturb any of the resulting charts, especially as each tympanic membrane is unique and will therefore not behave in a perfectly predictable manner. Despite the advantages of the method, only roughly 17% of audiologists will make use of tympanometry when treating patients, (Katz, 1994).

2.3 State of the Art

The latest experimental method for testing the tympanic membrane is done using Laser Doppler Vibrometers (LDVi), a non contact system that uses laser light to map tympanic response. The device detects the velocity of surfaces in a system and is then able to extract information relevant to factors such as position, (Cloud, 2005). The concept of LDVi has been in use for long before it was applied to the ear, (Castellini, 1998). The principle was first applied on cosmic scales for the sake of celestial research, and from there began to take on more microscopic tasks, (Cloud, 2005). Common uses for the technology outside of the medical field are quality control and tracking fluids, (Cloud, 2005). LDVi has shown in several tests to have the ability of eliminating the need for diagnosis by tympanometry, as it will provide the doctor with a plot of the tympanic membrane and the response, (Turcanu, 2006). The system has the ability to more closely indicate evidence such as the actual location on the tympanic membrane that a perforation may be present, or which bone in the linkage behind the membrane is not performing correctly, (Turcanu, 2006).

LDVi provides data to the user point by point when applied to a sample, (Castellini, 1998). When LDVi is applied then towards measuring the vibration response of a sample, it is helpful for the investigator to be able to collect multiple points at a time to receive a larger “field of view” of their data, (Castellini, 1998). The need for this information brought on Scanning Laser Vibrometers (SLVi) which will collect information from multiple points on a sample almost simultaneously, (Castellini, 1998). The technology has the ability to collect many points within a small area, so the

investigator is practically given an entire picture of the sample's response, (Castellini, 1998).

2.4 Interferometers

There are other methods that have the ability to provide data about TM response that will provide the user with different sets of data to use for further analysis.

Holographic interferometry is a hybrid optical testing method which has successfully been applied in the analysis of sample deformation, (Jones, 1983). The technique was pioneered in the 1960s as an expansion on interferometric techniques used to investigate test samples.

Interferometry is a practice which engages the properties of light to extract information relative to the change of the original light beam, (Meyers, 1991). In practice interferometry typically involves the splitting of a single light source into two different beams: a "reference" beam and an "object" beam, (Meyers, 1991). The wave properties of light are used to draw comparisons between the reference beam, which remains undisturbed between its source and detector, and the object beam, which is reflected off of a test surface and then recombined with the reference beam at the detector, (Meyers, 1991). The detector picks up the relative phase of the recombined beams and will see light and dark patterns form, (Meyers, 1991). The patterns are referred to as "fringes," and are caused by the waves canceling each other out so their net amplitude is 0, (Meyers, 1991).

As the measurement tool is a beam of light, the interferometer is accurate up to the wavelength of light being used, (Jones, 1983). For the case of measurements being conducted with visible light an interferometer has the ability to measure samples within an order of nanometers, (Jones, 1983). Each fringe produced by the interferometer is located a wavelength away from the next, (Jones, 1983).

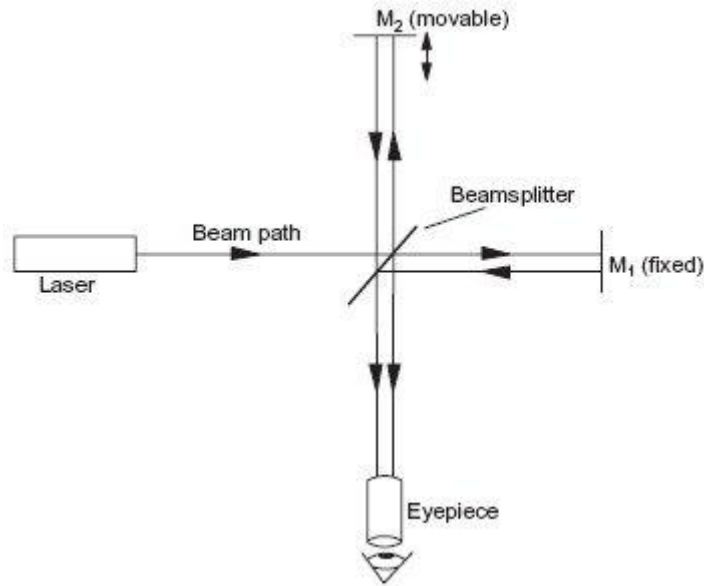


Fig. 2 - Example of an Interferometer (Answers.com)

Holography is the technique of recording three dimensional information of an object in an image by recording the light that is “scattered” by an object, (Mansuripur, 2002). Holograms record the intensities of light bouncing off of an object as well as the “phase information” embedded in the scattered light waves, (Meyers, 1991). A traditional photograph only records the intensities of the reflected light, (Meyers, 1991). For the purposes of analysis holograms have the ability to record much more information than a photograph, as they can produce three dimensional images which also enable the

viewer to investigate different perspectives of the object as well, (Tamir, 1983). A hologram, in effect, acts as a virtual diorama captured within a flat piece of film.

Holography is applicable in many different scenarios. Holograms have the ability to provide greater depths of field, preservation of dense packs of information and insight in to nano-scaled objects, (Tamir, 1983). As the hologram provides a virtual three dimensional image, the light wave information that is recorded does not have a particular focal point, allowing the sharpness of the hologram to be dependent on where the viewer would like to look, (Saxby, 2004). With this property also comes their ability to record large amounts of retrievable information, even on very small scales. Holograms can then use minimal space to virtually store large quantities of information which remain easily accessible.

Classical holography focused on the preservation of information relative to an object, requiring samples to remain completely still in the process of holographing, (Jones, 1983). Movement even on a miniature scale results in a blurring of the holograph, making the image worthless, (Jones, 1983). In the 1960s new techniques were developed combining principles of both interferometry and holography which made the movement of the sample object to be desirable for some cases of analysis, (Jones, 1983).

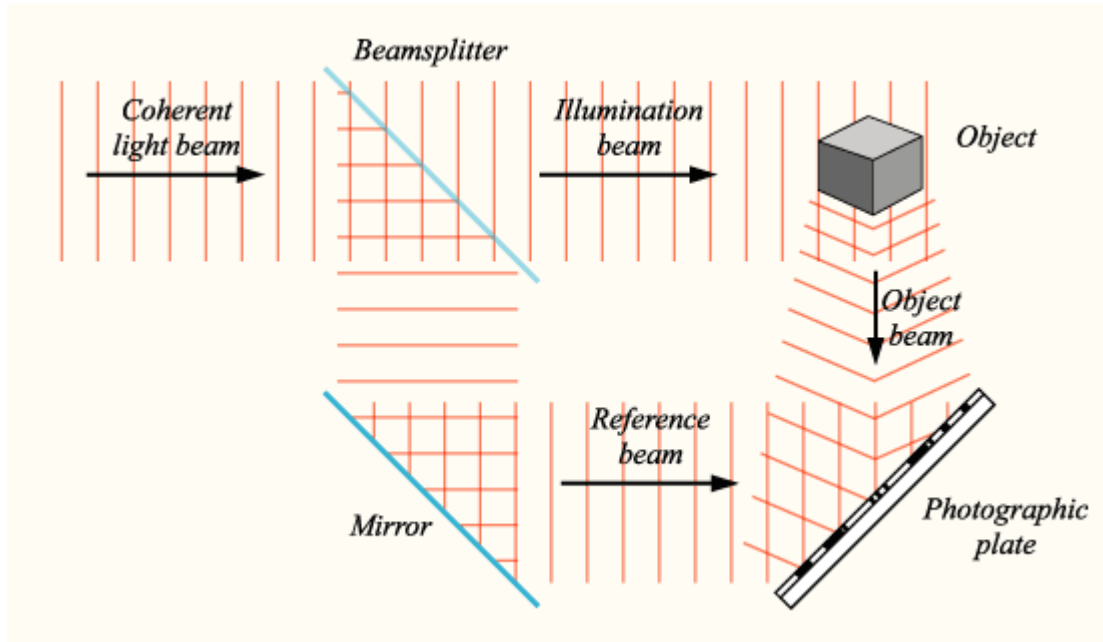


Fig. 3- Example of Principles of Holography (Stereoscopy.com)

Holographic interferometry uses the principles of interference and the tools of holography to collect data. The technique is used very effectively with samples that are in motion, and is capable of detecting minute changes in an object's shape, (Tamir, 1983). This makes the technique extremely effective in applications which involve observing vibrations on an object's surface, (Tamir, 1983). In most instances these vibrations are far too small and too quick to be observed by the bare eye. However, as holographic interferometry can detect changes on the order of nanometers it is entirely possible to display the effects of surface vibrations, (Tamir, 1983). Interference due to the vibrations on an object is displayed in the resulting images, and the visible interference indicates the pattern of vibration taking place, (Tamir, 1983).

In the cases of both interferometry and holography the light sources are commonly lasers, as they have the ability to emit light that is of uniform wavelength and

phase, (Meyers, 1991). This is especially important for the purposes of holography, as the light's coherence is critical to developing the hologram, (Meyers, 1991). In this case coherence is taken as meaning that the light used in the development of the hologram is one wavelength and travels in one direction only, (Meyers, 1991).

Laser stands for "Light Amplification by Stimulated Emission of Radiation," (Meyers, 1991). The first laser, developed by Theodore Maiman, managed to emit ruby colored light, (Essortment, 2002). The device was made of a ruby rod modified with semitransparent ends, and a flash bulb to excite photons inside of the ruby tube (howstuffworks.com, 2003). Excited photons that were able to escape the tube were monochromatic ruby, and collimated parallel with the direction of the tube, (howstuffworks.com, 2003). This is partly what separates lasers from light sources such as bulbs, (howstuffworks.com, 2003). Lasers emit collimated light that results in a concentrated, monochromatic, beam with uniform wave pattern, (howstuffworks.com).

This first laser could not emit light in a seamless beam however, due simply to the atomic properties of the ruby tube, (Essortment, 2002). Researchers began to suspect the properties of the ruby tube being responsible for the inconsistent behavior of the laser light and began to experiment with new mediums, (Essortment, 2002).

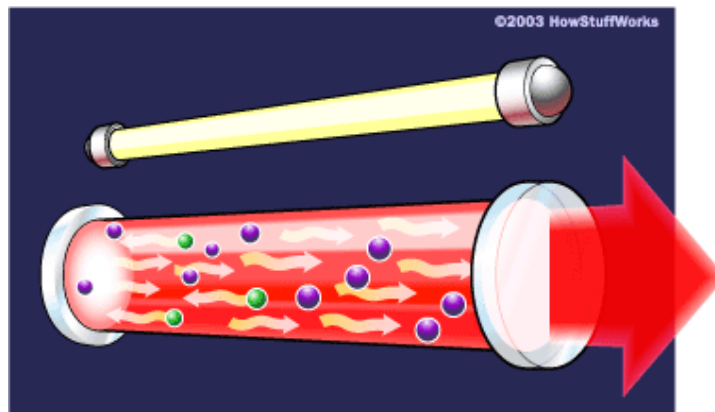


Fig. 4 - Ruby Laser Emitting Light, from <http://science.howstuffworks.com/laser.htm>

By the end of 1960 scientists were experimenting with gas-tube filled lasers, (Essortment, 2002). This laser, created by William Bennet, Donald Herriot and Ali Javan, became the dominantly used laser until the eighties, (Essortment, 2002). This laser would continuously emit light which enabled scientists to truly begin to discover the uses of laser technology, (Essortment, 2002). As laser technology improved the light that was emitted became more consistent, and developers have managed to be able to directly control output.

3 Methodology

3.1 Optical Head Development

Our task, mechanically, was to design a self-standing enclosure for specific optical components of an interferometer. The components are shown in Fig. 5 and include the CCD camera (A), beam splitter cube (B), reference beam with positioning capabilities (C), object beam with positioning capabilities (D), and the lens and aperture (E).

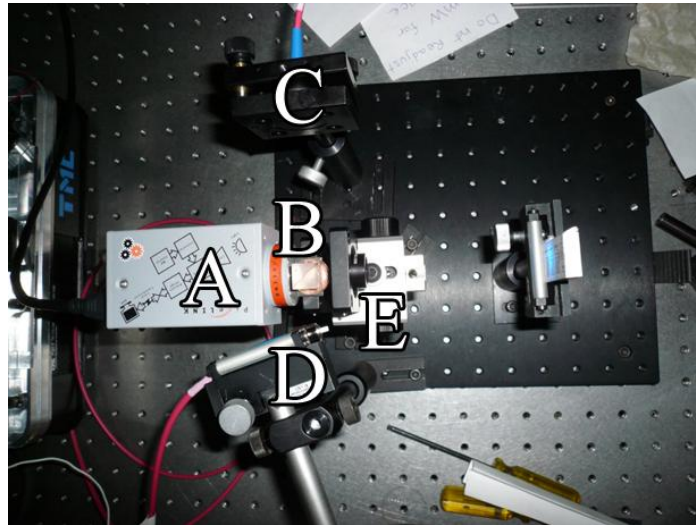


Fig. 5 - Breadboard Configuration

The group approached the task by brainstorming a variety of solutions. The top three included a cylindrical camera-like enclosure, a plate design for post-mounts to attach to, and a box-type enclosure.

The basis of the cylindrical design was to come up with an enclosure that resembled a camera lens. The main advantages to this were its compact size and attractive styling. The design made use of the adjustable lens tubes for focusing purposes and made the assumption that the reference beam could be held perpendicular to the

optical axis. Driven by time constraints, however, the cylindrical design did not have a mount for the illumination beam. Upon fabrication of the prototype, the perpendicularity of the reference beam was found to produce an undesirable amount of secondary fringes. This particular finding led us to investigate the degrees of freedom that were necessary to produce acceptable images. Fig. 6 shows the manufactured prototype.



Fig. 6 - Cylindrical Design

The plate design was our way to experiment with different components and isolate necessary degrees of freedom. One of our main interests was emulating the method of illumination utilized in otoscopes by the way of illumination fibers. We acquired a rigid fiber to test the feasibility of using illumination fibers as light guides. Our research found that the use of fibers randomly dispersed the intensities of the light, producing a non-uniform illumination and undesirable images. Additionally, it was found that the reference beam can not be confined to any specific degrees of freedom, therefore 6 degrees of freedom were necessary. The illumination beam must also be centered height-wise on the optical axis to ensure uniform illumination and the angle

made by the beam with the optical axis must be as small as possible (ideally 0 degrees).

Fig. 7 shows the plate design in its test configuration.

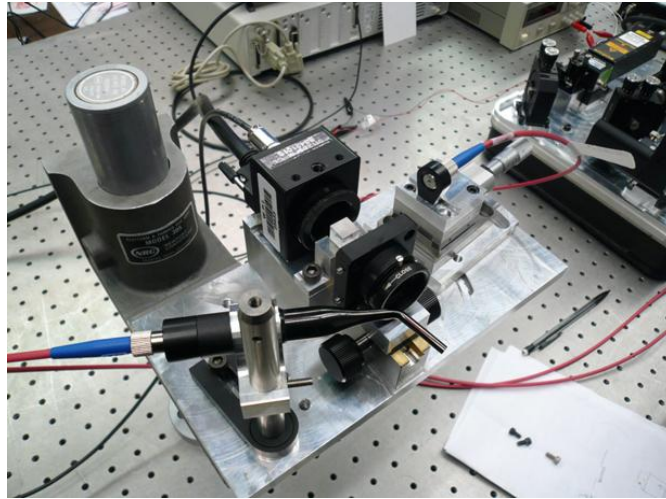


Fig. 7 - Plate Design

The box design creates a compact, enclosed unit for the components to attach to. This design allows the user to easily transport the device without taking the time to meticulously align each component. Additionally, the enclosure provides a means of blocking any stray light from affecting the quality of the images. The placement of the optics inside the enclosure had to allow for the following range of working distances for different fields of view. Different fields of view are necessary to accommodate the varying size of the tympanic membrane from species to species. These limiting distances ultimately defined the maximum allowable size of the enclosure.

Distance from CCD Chip to Lens (mm)	Distance from Lens to Object (mm)	Field of View (mm)
30.35	89.76	9.84
34.30	78.85	8.53
38.92	69.92	6.70
29.70	96.19	11.18

Table 1 - Working Distance Constraints

By the time the first version was ready to be manufactured, the enclosure had the following features. First, the base of the enclosure for mounting remained relatively thick (approximately 1 inch) to stop as much deformation from occurring. Second, it was found that by running the reference beam through a collimator the secondary fringes disappeared entirely. Therefore, the 6 degrees of freedom mounting plate was replaced by a simpler collimator assembly. Finally, the illumination beam reflects off of a mirror to achieve a relatively small angle with the optical axis while maintaining uniform illumination. Fig. 8 shows the first version being used in a real world environment at the Massachusetts Eye and Ear Infirmary.

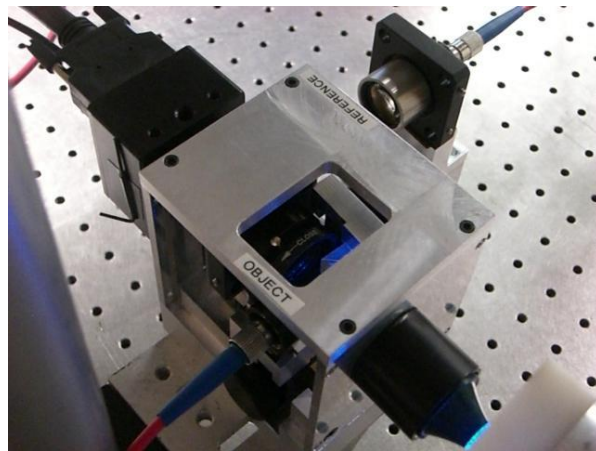


Fig. 8 - Box Design

The delivery of the first version of the box design was heavily driven by strict time constraints and even though it was providing excellent images for the doctors, there were improvements that could be made.

The orientation of the camera and speculum were found to have a noticeable dependency with how their mounting plates were assembled. This dependency skewed the optical axis at times, making it difficult to acquire acceptable images. To fix this problem, the plates are now mounted to the top of the base rather than from the side.

To make aligning each component as easy as possible, alignment slots were integrated into each component that mounted to the base. These components included the camera plate, speculum plate, beam splitter cube holder, collimator mount, and mirror plate. These slots encourage each part to remain aligned with one another and also promote consistent assembly of the optical head.

At times, the mirror produced a visible line on the image from the reflection of light off its edge. In an attempt to eliminate that from occurring, the following changes were made. The mount for the fiber was given the ability to move along the optical axis. The positioning plate was replaced by a compact rotational stage to allow for the mirror to be placed as close to the optical axis as possible without interfering with the field of view of the image. The estimates of the angle made between the optical axis and illumination beam are approximately 5 to 9°.

These changes did not affect the overall length of the optical head and the new version can still achieve the necessary working distances. The second version was sent out to be manufactured and currently resides in the CHSLT lab in Higgins. Fig. 9 is a rendered picture of the assembly model in Pro-Engineer with its cover lifted.

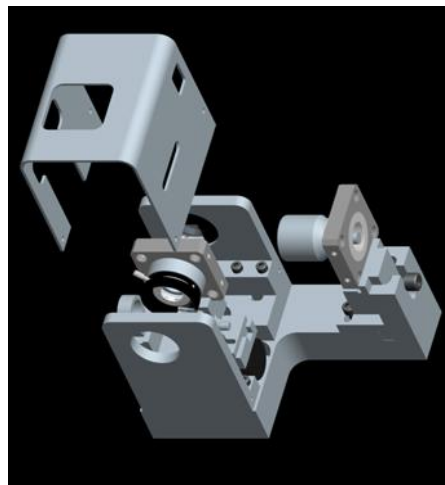


Fig. 9 - Refined Box Design

3.2 Validation of Performance

In order to validate the performance of the system, it was necessary to verify that the images gathered by the device were in fact representative of what was occurring. To do so, a known geometry with predictable characteristics was required to compare and make conclusions with obtained experimental results. Since the geometry of the tympanic membrane is extremely complex, the object of interest was simplified to a thin circular plate of copper with a thickness similar to that of a tympanic membrane (0.001 inches thick). With these carefully chosen geometries and material properties, the frequencies for the modes of vibration we were interested in observing fell within the response range of the human ear.

3.2.1 Analytical Results

The first step was to develop an analytical model to approximate the frequency of vibration for the first 6 modes and predict the corresponding shape of each mode. In this section, all of the following assumptions and equations (equation 3.1 through equation 3.13) were compiled from derivations contained in the references McLachlan (1961) and Reddy (1999).

The boundary conditions in this situation are assumed to be clamped at the edges and the plate is assumed to be undergoing free (natural) vibration. With these assumptions, the deflection can be represented as a periodic function. Therefore, by applying the deflection equation to the equation of motion of an isotropic plate, equation 3.1 results:

$$D\nabla^2\nabla^2 W + k W - I_p \omega^2 + I_R \omega^2\nabla^2 W = 0 \quad (3.1)$$

Where:

- k is the modulus of elasticity of the substrate the plate rests on
- D is the modulus of rigidity of the plate
- I_p is the principal inertia of the plate
- I_R is the rotary inertia of the plate
- W is the deformation equation
- ω is the frequency of vibration

IR can be neglected because the term contributes very little to the fundamental frequencies and will make solving for the frequencies rather difficult. Simplifying the equation of motion yields the following:

$$\left(\nabla^4 - \beta^4\right) W = 0 \quad \text{where} \quad \beta^4 = \frac{I_p \omega^2 - k}{D} \quad (3.2)$$

The solutions to equation 3.2 can be found by factoring and separating it into the following equations:

$$\nabla^2 W_1 + \beta^2 W_1 = 0 \quad \text{and} \quad \nabla^2 W_2 - \beta^2 W_2 = 0 \quad (3.3)$$

It is assumed that the solution to equation 3.2 can be characterized by the general Fourier series shown in equation 3.4.

$$W(r, \theta) = \sum_{n=0}^{\infty} \left(W_n(r) \cos(n\theta) \right) + \sum_{n=0}^{\infty} \left(W_n^*(r) \sin(n\theta) \right) \quad (3.4)$$

Plugging in equation 3.4 as the solution of the PDE yields the following two pairs of identical equations for W_n and W_n^* :

$$\begin{aligned} \frac{d^2 W_{n1}}{d r^2} + \frac{1}{r} \left(\frac{d W_{n1}}{d r} \right) - \left(\frac{n^2}{r^2} - \beta^2 \right) W_{n1} &= 0 \\ \frac{d^2 W_{n2}}{d r^2} + \frac{1}{r} \left(\frac{d W_{n2}}{d r} \right) - \left(\frac{n^2}{r^2} - \beta^2 \right) W_{n2} &= 0 \end{aligned} \quad (3.5)$$

One can numerically solve the two pairs of equations in equation 3.5 by use of Bessel Functions and can be expressed as the following:

$$\begin{aligned} W_{n1} &= A_n J_n(\beta r) + B_n Y_n(\beta r) \\ W_{n2} &= C_n I_n(\beta r) + D_n K_n(\beta r) \end{aligned} \quad (3.6)$$

Where:

- J_n is a Bessel Function of the first kind where it is finite at the origin, resembling a decaying periodic function
- Y_n is a Bessel Function of the second kind where it is infinite at the origin, resembling a decaying periodic function
- I_n is a Modified Bessel Function of the first kind where it is finite at the origin and grows exponentially
- K_n is a Modified Bessel Function of the second kind where it is infinite at the origin and decays exponentially

Combining equation 3.6 into equation 3.4 yields the general form of the solution shown in equation 3.7

$$\begin{aligned} W(r, \theta) &= \sum_{n=0}^{\infty} A_n J_n(\beta r) + B_n Y_n(\beta r) + C_n I_n(\beta r) + D_n K_n(\beta r) \cos(n\theta) \\ &+ \sum_{n=1}^{\infty} A_n^* J_n(\beta r) + B_n^* Y_n(\beta r) + C_n^* I_n(\beta r) + D_n^* K_n(\beta r) \sin(n\theta) \end{aligned} \quad (3.7)$$

Where A_n , B_n , C_n , and D_n are all coefficients used to determine mode shapes by applying the appropriate boundary conditions.

The terms including the Modified Bessel Functions, Y_n and K_n , are neglected as they would result in infinite values of deflection at the center of the membrane. Additionally, assuming that the solution is symmetric, any terms containing $\sin(n\theta)$ are neglected as well. This results in the following equation:

$$W_n(r, \theta) = \left(A_n J_n(\beta r) + C_n I_n(\beta r) \right) \cos(n\theta) \quad (3.8)$$

Equation 3.8 is the general form of the equation. The following boundary conditions for a clamped circular plate must be considered:

$$W_n = 0 \quad \text{and} \quad \frac{\partial}{\partial r} W_n = 0 \quad \text{at} \quad r = a \quad \text{for any } \theta$$

Applying these boundary conditions to equation 3.8 yields:

$$\begin{bmatrix} J_n(\lambda) & I_n(\lambda) \\ J_n'(\lambda) & I_n'(\lambda) \end{bmatrix} \begin{bmatrix} A_n \\ C_n \end{bmatrix} = \begin{bmatrix} 0 \\ 0 \end{bmatrix} \quad (3.9)$$

Where $\lambda = \beta r$ evaluated at $r = a$ and the ` on the Bessel Functions represents differentiation with respect to βr . Upon setting the determinant of the coefficient matrix in equation 3.9 to zero yields the following:

$$J_n(\lambda) I_{n+1}(\lambda) + I_n(\lambda) J_{n+1}(\lambda) = 0 \quad (3.10)$$

The roots λ can be approximated by using the asymptotic series for the Bessel functions shown in equation 3.11:

$$\lambda_{n,m} = \theta - \frac{4n^2 - 1}{8\theta} \left(1 + \frac{1}{\theta} + \frac{28n^2 + 17}{48\theta^2} + \frac{3(4n^2 - 1)}{8\theta^3} + \frac{83n^4 + 54.5n^2 + 161.19}{120\theta^4} + \dots \right)$$

$$\text{Where } \theta = \frac{(2m + n)\pi}{2} \quad \text{for } m \geq 1 \quad (3.11)$$

Additionally, m is the rank of the root and n is the order of the root. Now, looking back at the definition of β in equation 3.2, simple algebra can be used to develop an equation for determining the frequencies:

$$\omega^2 = \frac{D\beta^4 + k}{I_p} \quad (3.12)$$

Assuming that the membrane foundation is rigid ($k = 0$) and substituting β with λ/a results in the final equation for determining the frequency of vibration:

$$\omega = \frac{\lambda^2}{a^2} \sqrt{\frac{D}{I_p}} \quad (3.13)$$

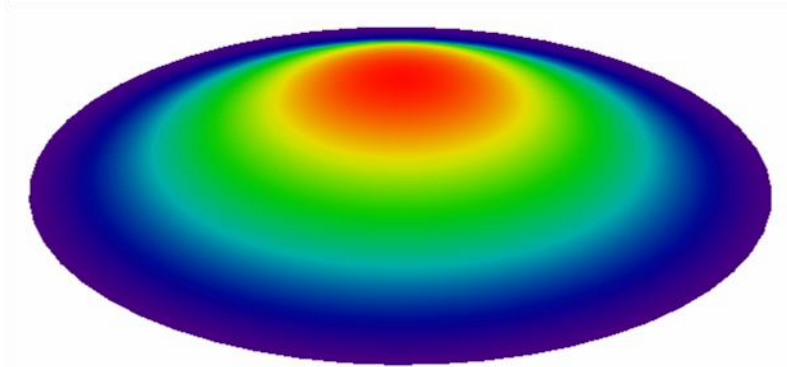


Fig. 10 - First Mode of Vibration Obtained with MathCAD

Additionally, by applying specific shape functions to the derived equations, one can predict the shapes of the desired mode. Upon evaluating the equations for modes 1 through 6, the frequencies and shapes were obtained. Fig. 10 shows the first mode shape given by the analytical model. For a detailed representation of the MathCAD file used to generate these frequencies, refer to the included CD.

3.2.2 Computational Results

To verify the consistency of the experimental results of an oscillating thin circular membrane the problem was solved computationally using finite element method. The oscillating membrane was modeled in the finite element program Abaqus/CAE version 6.7. We found that the computational approach verified the experimental results with in some margin of error.

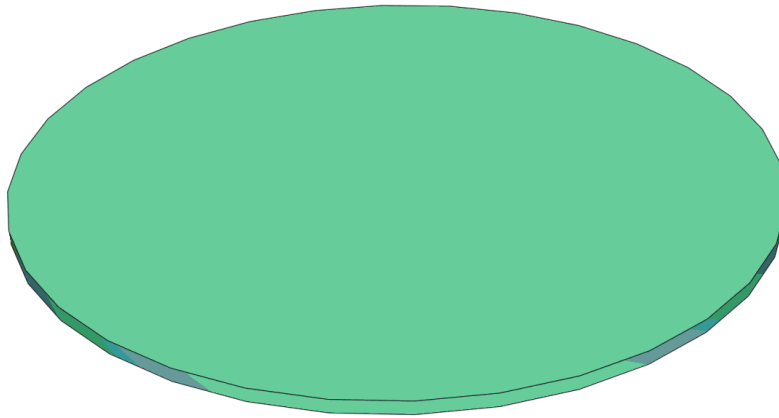


Fig. 11 - 3D Deformable Solid Thin Membrane

The membrane was modeled as a 3D deformable solid with a diameter of 1 cm and a thickness of 0.0254 mm (see Fig. 11). The material properties were entered for copper with a density of 8960 kg/m^3 , a Young's Modulus of 110 GPa and a Poisson's ratio of 0.343. A solid, homogeneous section was created and assigned to the entire membrane. A boundary condition was placed on the circumference of the membrane constraining movement in the x, y and z directions.

In Abaqus CAE analyses are done in steps and each step defines a specific output. One can easily analyze the static and dynamic behavior of a system in one model by creating one step for the static analysis and one step for the dynamic analysis. Since only the dynamic behavior of the thin membrane is of concern only one step is needed.

The step required for the analysis is a frequency extraction step. Abaqus offers several different methods to extract the frequencies. The Lanczos eigensolver method was chosen for this because it is a general purpose method that covers most cases. The disadvantage is that it is a less efficient calculation than the alternatives but since only six modes are needed, the added time is acceptable.

One of the most important aspects of a good FEA model is its mesh. Small changes in mesh sizing and orientation can produce drastically different results especially for dynamic analyses. These values must be chosen very carefully to ensure that the results are accurate. It was found that the mesh size needed to be refined using two different methods in order to achieve convergence. The first method of refinement uses partitions to divide the membrane into more layers (see Fig. 12). This technique has a linear effect on the number of elements in the model. It was found that as the membrane was divided into more layers, the modal frequencies increased towards convergence. Four layers is a good compromise between computation time and accuracy of the result.

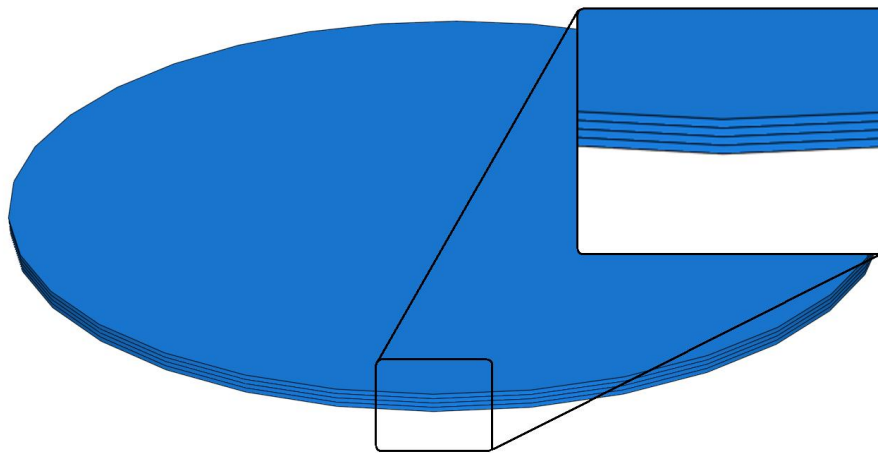


Fig. 12 - A Closer Look at Partitions

The second method for mesh refinement that was used was the adjustment of the seed size. In Abaqus CAE the number of elements that comprise a body is controlled by the length of element edges that fall on geometrical edges in the body. This distance is called the seed size. In this model, the number of elements is proportional to the inverse of the seed size squared. Refining the seed size had the effect of decreasing the modal frequencies towards convergence. Using the two methods described, the mesh was refined until a converged solution was obtained (see Fig. 13).

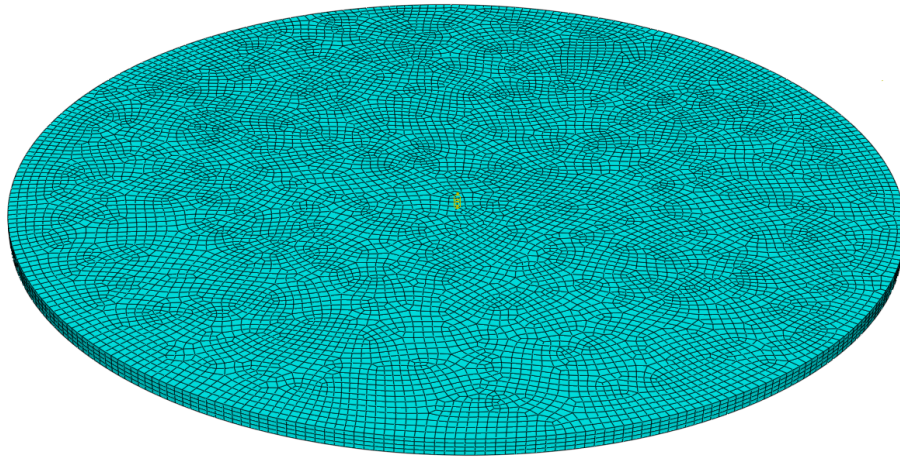


Fig. 13 - Refined Mesh

Results were obtained for the first six modes of vibration. For each of the six modes a deformed contour plot of the mode shapes was created. The frequency and the mode shape were then used to validate the data that was obtained from the experimental and computational methods.

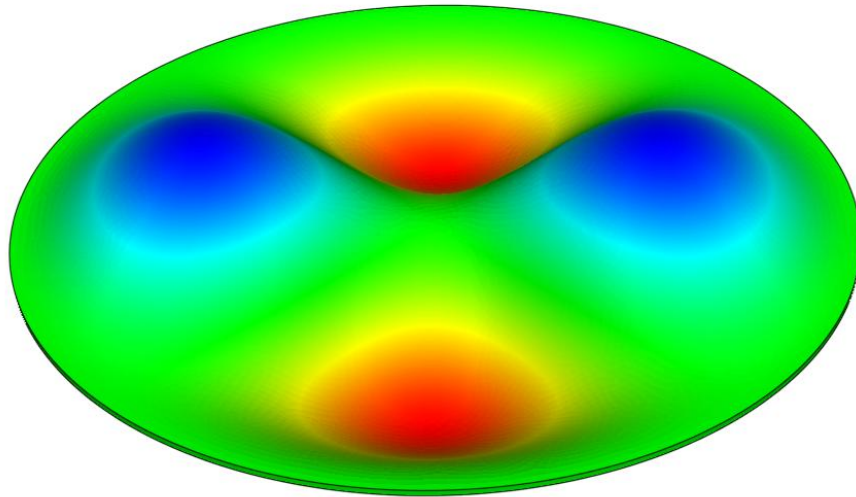


Fig. 14 - Fourth Mode Deformed Contour Plot

3.2.3 Developing a Perfect Membrane

Before results were obtained using experimental methods a near perfect brass membrane was manufactured. This proved to be a fairly difficult task because the membrane, in order to respond within the audible range, had to be approximately 0.001 inches thick. Creating a membrane with uniform thickness, good surface finish and uniform boundary conditions required a level of precision that was not required on other parts that were manufactured.

A number of different approaches were considered for creation of the membrane, each having its own distinct advantages. The first method was to machine it from a single piece of brass. A circular pocket was milled out from a single stock leaving only a thin layer of material at the bottom. The advantage of this method was that it had uniform boundary conditions assuming that there were no internal stresses that resulted from the machining. Ultimately the approach failed because the membrane would repeatedly shear

off as the mill approached the required depth. It was also very difficult to control the surface finish.

A more practical solution to the problem was determined to be the use of a thin metallic foil clamped by a separate mechanism (see Fig. 15). Commercially available foils have the advantage over machined stock in that the thickness is very precise and the surface finish is consistent. Aluminum and Copper foils of various thicknesses were purchased.

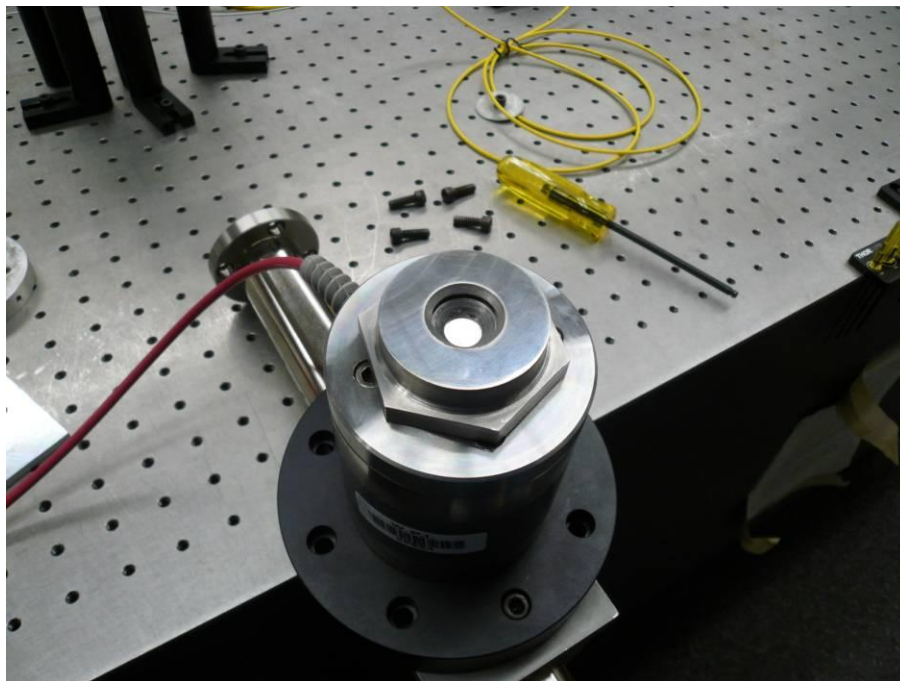


Fig. 15 – Foil Clamping Mechanism Mounted onto the Piezo

The foil had to be secured in a way that ensured uniform boundary conditions that resembled those in the analytical and computational models. To do this, a device was designed and manufactured out of steel that clamped the foil between two surfaces. The base of the device was bolted onto the piezo that was used for excitation. This provided the surface that the foil was laid on and had a 10 mm hole in the middle. A circular part, guided by pins to prevent rotation, was then rested on top of the foil. The part had a

raised surface around the edge of a hole in the center. The raised surface clamped the foil to the base. To apply uniform pressure to the device a thrust bushing was placed on top of the circular clamp and a nut pressed the assembly together. Since the stiffness of the steel device is significantly greater than that of the membrane that it holds, its deformations could be ignored.

Initial results that were obtained using the device showed that the pressure that was applied to the foil was not uniform. This was confirmed by a visual inspection of the foil which showed that it had been deformed on some areas but was left untouched in others. This can easily be explained by manufacturing flaws. Since the foil being clamped is only 0.001 inches thick, even the smallest of imperfections can be enough to cause problems. The precision of the machines that the parts were initially made on was only 0.0001 inches and this does not account for tool vibrations, deflection or poor surface finish. More importantly, the angular tolerance between the two surfaces is increased because the parts are not always loaded into their fixtures perfectly before machining.

To improve the uniformity of pressure, a secondary manufacturing technique was used. Surface grinding is a technique that is commonly used to achieve the flatness on parts that cannot be had using conventional machining techniques. The raised surface of the circular clamp was ground off by a slight amount. This ensured that the ground surface was parallel to the opposing surface that mated to the thrust bushing. The solution proved to be effective along with the use of the thicker foils.

Despite the improvements that were made to the clamping device, great care was needed for the preparation. Since the surface of the foil was shiny and metallic, it did not provide the best conditions for imaging. The foil was prepared in several different ways

in order to determine what provided the best quality images. To reduce the glare, the foil surface was sanded using 600 grit sand paper. The quality of the images was improved to a degree but they were still not acceptable for use as a comparison. Other foils were painted with a thin layer of flat white paint. This technique is also used by MEEI to prepare the tympanic membranes for testing. Using this method the image quality was more than acceptable. The paint does add some thickness of material of unknown properties but it was assumed to be negligible for the experiments purposes.

Once prepared, it was very important that the foil be loaded into the clamp carefully. Any kind of crease in the foil showed to have an affect on the results. Fig. 16 shows the deformations on a creased foil as a result of clamping.



Fig. 16 - Deformations on a Creased Foil Due to Clamping

The image was taken using a holographic technique called time averaging. The greatest deformations occur at the crease of the membrane and can be seen as fringes on

the image. When loaded properly, the membrane showed a uniform ring of deformation on the edge that it was clamped. The copper foil did not crease as easily as the aluminum did so it was selected for the test material.

3.2.4 Experimental Results

Painted copper foil 0.001 inches thick was clamped in the manufactured device and measured with the LHO to determine the mode shapes and frequencies of vibration when excited. The excitation was provided by a piezo that was driven by a frequency generator. Additionally, a 512 nm wavelength, 20 mW laser was used for illumination and monochromatic digital video camera was used for imaging.

Starting with an amplitude of 10 volts, the frequency was continuously increased from 100 Hz until the first mode of vibration was reached. The amplitude was adjusted so that the deformations were in the range of the LHO. The frequency was recorded and the image, showing the mode shape of vibration, was captured (see Table 4). The procedure was repeated for the first six modes of vibration. Table 2 contains the data acquired from this membrane test.

Material	Thickness (inches)	Coating
Copper	0.001	White Paint
Mode	Frequency (Hz)	Amplitude (Volts)
1	2150	5.4
2	4100	7.7
3	4470	2.7
4	6600	2.8
5	6630	2.7
6	7290	2.3

Table 2 - Membrane Test Data

3.2.5 Comparing Results

The analytical and experimental results were used to validate the LHO measurements. All methods provided the shapes and frequencies for the first six modes of vibration (see Table 4 and Table 4).

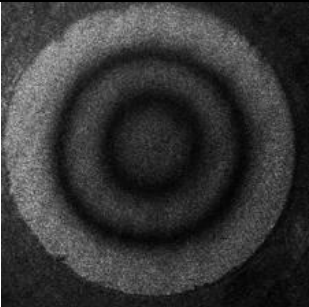
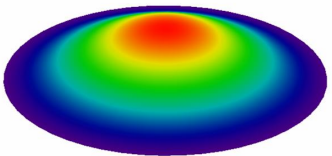
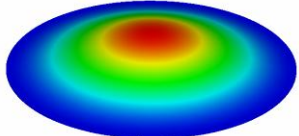
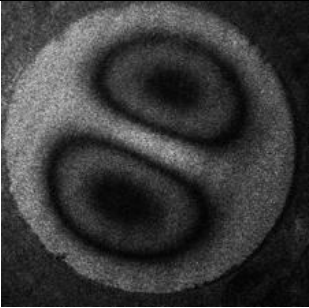
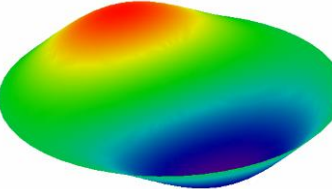
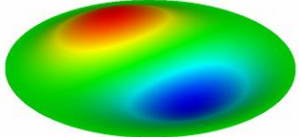

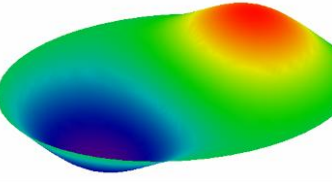
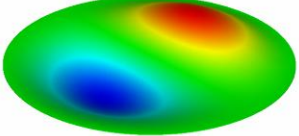
Mode	Experimental Copper Foil: 0.001" Thick Painted	Analytical	FEA
1	 2150 Hz	 1830.6 Hz	 1876.6 Hz
2	 4100Hz	 3812.2 Hz	 3899.3 Hz
3	 4470 Hz	 3812.2 Hz	 3899.3 Hz

Table 3 - Mode Shapes and Frequencies for Modes 1 through 3 Taken from Experimental, Analytical and Finite Element Methods

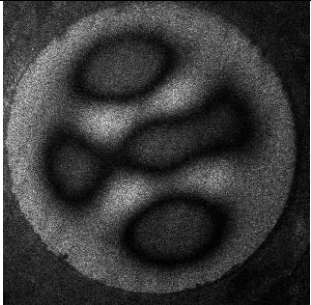
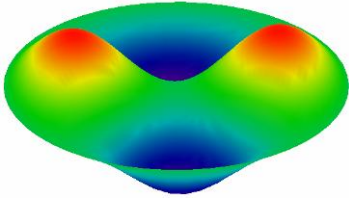
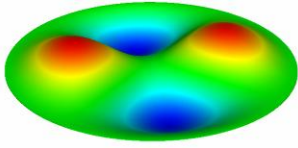
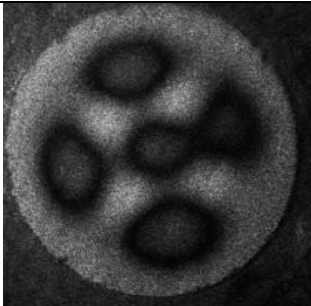
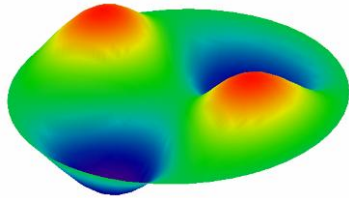
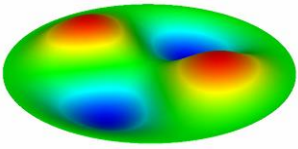
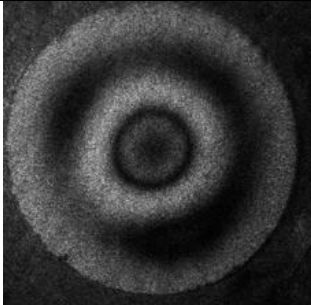
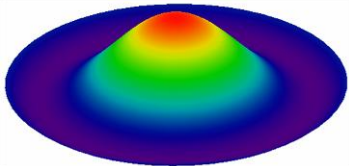
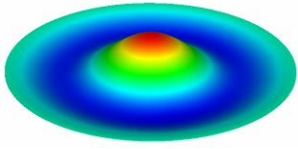
Mode	Experimental Copper Foil: 0.001" Thick Painted	Analytical	FEA
4	 6600 Hz	 6256.3 Hz	 6381.8 Hz
5	 6630 Hz	 6256.3 Hz	 6381.8 Hz
6	 7290 Hz	 7128.6 Hz	 7329.9 Hz

Table 4 - Mode Shapes and Frequencies for Modes 4 through 6 Taken from Experimental, Analytical and Finite Element Methods

Mode	Analytical	Computational
1	17.45%	14.57%
2	7.55%	5.15%
3	17.26%	14.64%
4	5.49%	3.42%
5	5.97%	3.89%
6	2.26%	0.54%

Table 5 - Experimental Results Percent Error

The error between the experimental and other two methods was calculated (see Table 5). At most, the experimental deviates from the analytical by 17.45 percent for the first mode and the computational by 14.64 percent for the third mode. The error that occurred can probably be attributed to several sources. The models in both the analytical and computational were greatly simplified. The force that was applied to the foil was ignored and it was assumed to be a thin cylindrical slice with a zero displacement boundary condition at the circumference. The assumptions that were made do not take into account the affects that uneven pressure has on the results. Additionally, the paint on the membrane might have been uneven, and it added extra unaccounted mass to the membrane. The error was minimized at higher modes with a minimum of 2.26 percent with the analytical and 0.54 percent with the computational, both occurring at the sixth mode. Despite the error, the results were a good indication that the LHO was working as intended.

4 Results

The Laser Holographic Otoscope was delivered to the Massachusetts Eye and Ear Infirmary (MEEI) in Boston, Massachusetts to conduct tests on true TM samples. The system was installed in their laboratory in a sound proofed room and fully integrated with the appropriate medical equipment. The device was calibrated for the doctors after being installed in the lab ensuring good image quality for all results.

Doctors prepared several different sample types for use with the device, among which were that of chinchilla, cat and human TMs. The test samples were acoustically excited using a speculum designed specifically to direct sound at the test samples. The mode shapes of vibration were able to be captured by the device and the doctors were able to observe the patterns that were induced.

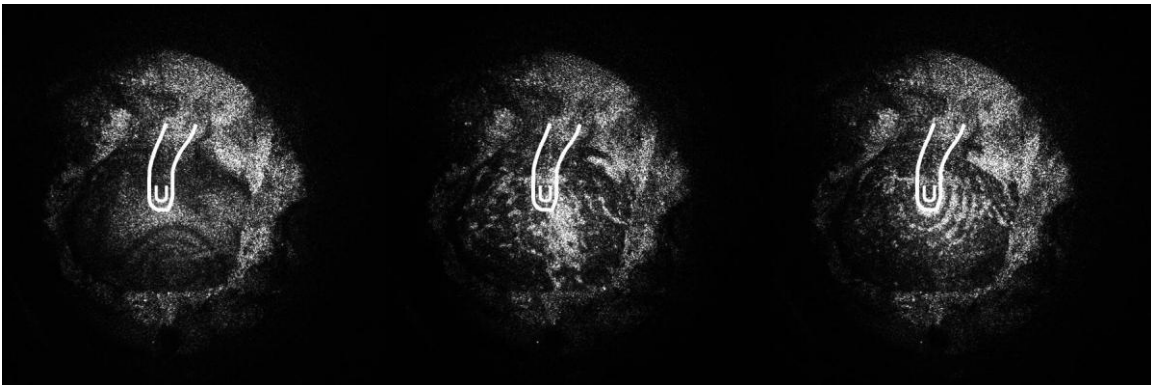


Fig. 17 - Live Chinchilla TM Excited at: 600Hz -23dBV (101dBSPL), 10 kHz - 29dBV (127 dBSPL), 22 kHz - 39dBV (108dBSPL)

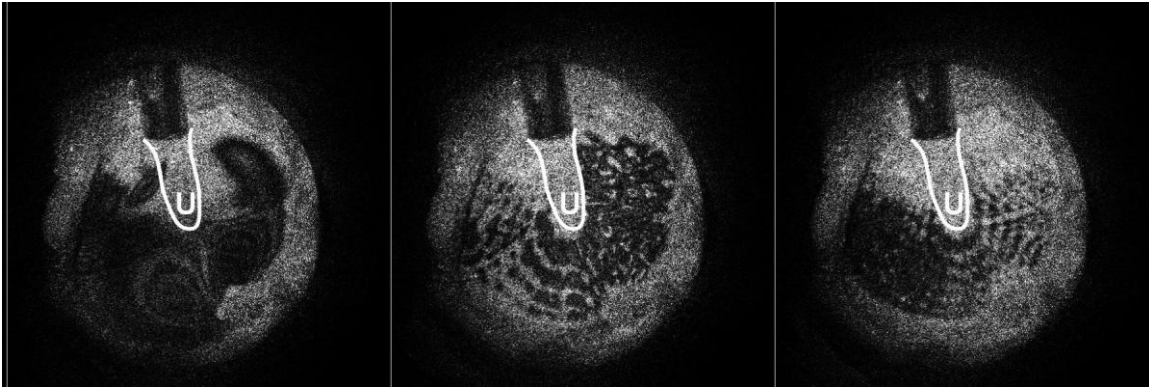


Fig. 18 - Post Mortem Chinchilla TM Excited at 500Hz - 46dBV, 10 kHz - 34 dBV, and 22kHz - 29 dBV

Images were collected such as in Fig. 17 and Fig. 18. The doctors were able to retrieve information on the behavior of the TM at levels that have never before been observed. Specifically, the doctors were able to characterize the response of the TM at frequencies above that of 10 kHz. This type of data will lead to much greater understanding of the TM and its function.

Doctors reported that the device was proving extremely effective for their testing purposes. The testing has been affected by the presence of vibrations near the testing laboratory but the physicians report that this is not due to the device's design or construction but rather from the environment which the device is in. The doctors also report that the use of the device is not overly complicated. Images can be brought in and out of focus with relative ease, and integration of the optical head with test samples can be performed with consistency.

5 Conclusions

Tests conducted in the Center for Holographic Studies and Laser micro-mechaTronics within WPI have validated the reliability of the system in its ability to collect clear images with nanometer resolution of foil samples excited with piezo actuators to produce vibratory response. The final design provided real-time images which corresponded directly with predictions of sample mode shapes from analytical models and finite element models.

The device is being used by doctors to investigate different species of tympanic membranes, including that of humans. Medical doctors currently experimenting with the device and are pleased with the results they are obtaining. The system is collecting data on tympanic membrane excitation that had previously been impossible with traditional method for tympanic investigations.

Feedback has also indicated that improvements in the device could be made with respect to the device's ability to adjust its illumination intensities for the object and reference beams. The doctors also suspect that there are portions of the resulting images that are being lost due to the capacity of resolution that the system can obtain. It is possible that there is information being lost as it is located between pixels.

The doctors feel that the future potential for the device in the medical community is high. The current device is effectively collecting information that should provide physicians in the future with information that will be necessary to better diagnose hearing conditions in human patients.

6 References

- About.com. "Lasers - The History of Lasers." (2008).
<http://inventors.about.com/od/1startinventions/a/laser.htm>
- Carlson, Paul F. Introduction to Applied Optics for Engineers. (1977). New York, New York: Academic Press.
- Castellini, P., Revel, G.M., and Tomasini, E.P. (1998). Laser Doppler Vibrometry: A Review of Advances and Applications. *The Shock and Vibration Digest*, 30. Retrieved March 25, 2008 from <http://svd.sagepub.com/cgi/reprint/30/6/443>.
- Cloud, Gary (2005) Back to Basics. Optical Methods in Experimental Mechanics. Part 17: Laser Doppler Interferometry. *Experimental Techniques* 29 (3). Retrieved March 25, 2008 from <http://www.blackwell-synergy.com/doi/pdf/10.1111/j.1747-1567.2005.tb00216.x?cookieSet=1>.
- Consortini, Anna. Trends in Optics: Research, Developments and Applications. (1996). San Diego, California: Academic Press Inc.
- Csillag, András. Atlas of the Sensory Organs: Functional and Clinical Anatomy. (2005). Totowa, New Jersey 07512: Humana Press.
- Essortment: Information and Advice you Want to Know. "A Technical History of the Laser." (2002). http://www.essortment.com/historyoflaser_rsny.htm
- Furlong, Cosme, Rosowski, John J., Hulli, Nesim, & Ravicz, Michael E. Preliminary Analyses of Tympanic-Membrane Motion from Holographic Measurements. *Strain*, 1-32.
- Howstuffworks.com. "How Lasers Work." (2003).
<http://science.howstuffworks.com/laser.htm>
- Jones, Robert. Holographic and Speckle Interferometry: A Discussion of the Theory, Practice and Application of the Techniques. (1983). Great Britain: J. W. Arrowsmith Ltd.
- Katz, Jack. Handbook of Clinical Audiology: Fourth Edition. (1994). Baltimore, Maryland: Williams & Wilkins.
- Mansuripur, Masud. Classical Optics and its Applications. (2002). United Kingdom: Cambridge University Press

- McLachlan, N.W. Bessel Functions for Engineers. (1961). Oxford University Press. Amen House, London E.C.4.
- Meyers, Robert A. Encyclopedia of Lasers and Optical Technology. (1991). San Diego, California: Academic Press Inc.
- Reddy, R.N. Theory and Analysis of Elastic Plates. (1999). Taylor and Francis. 325 Chestnut Street, Philadelphia, PA 19106.
- Rosowski, John J. and Merchant, Saumil, N. (Eds.). (2000). *The Function and Mechanics of Normal, Diseased and Reconstructed Middle Ears*. Kugler Publications.
- Saxby, Graham. Practical Holography. (2004). Retrieved 4/20/2008 from <http://books.google.com>.
- Schubert, E.D. Hearing: Its Function and Dysfunction. (1980). New York, New York: Springer-Verlag.
- Tamir, Theodor. Engineering Optics. (1983). Tokyo, Japan: Keigo Iizuka.
- Turcanu, D., Mărtu, D., Dalhoff, E., Gummer, A.W. “Laser Doppler vibrometry: a new tool for diagnosing hearing loss with an intact eardrum.” (2006). Universitatea de Medicină și Farmacie Gr.T. Popa Iași, Facultatea de Medicină Dentară, Spitalul Clinic de Recuperare. Retrieved March 24, 2008 from <http://www.ncbi.nlm.nih.gov/sites/entrez>.

7 Appendix A: Contents of Enclosed CD

Final Poster Folder

Contents include the MQP poster: PowerPoint format

Final Report Folder

Contents include the MQP report: PDF and Word Document formats

Finite Element Files Folder

Contents include the output database file that solves for the frequencies of vibration.

Gibbs Cam Files Folder

Optical Head Folder

Contents include cam files for manufacturing the first iteration of the box design.

Membrane Clamp Folder

Contents include cam files for manufacturing the membrane clamp

MathCad Files Folder

Contents include the MathCad file that solves for the frequencies of vibration.

Pro-E Files Folder

Optical Head Folder

Contents include the Pro-E files for the final iteration of the box design

Membrane Clamp Folder

Contents include the Pro-E files for the membrane clamp